

MODELING TSUNAMI SOURCES AND THEIR PROPAGATION IN THE ATLANTIC OCEAN FOR COASTAL TSUNAMI HAZARD ASSESSMENT AND INUNDATION MAPPING ALONG THE US EAST COAST ¹

Stéphan Grilli², Annette R. Grilli², Babak Tehranirad³ and James T. Kirby³

ABSTRACT

Numerical simulations are performed to develop tsunami inundation maps for the US east coast (USEC), as envelopes of surface elevations caused by the probable maximum tsunamis (PMTs) in the Atlantic Ocean basin. These PMTs are triggered by various sources, identified from historical records or hypothetical, including : (i) near-field submarine mass failures (SMF) on or near the continental shelf break; (ii) an extreme hypothetical M9 seismic event occurring in the Puerto Rico Trench; (iii) a repeat of the historical 1755 M9 (Lisbon) earthquake occurring in the Madeira Tore Rise; and (iv) large scale volcanic flank collapses (80 and 450 km³) of the Cumbre Vieja Volcano (CVV) on La Palma, in the Canary Archipelago. Tsunamis caused by: (1) earthquakes, are obtained from the estimated coseismic seafloor deformation; (2) SMF sources, modeled as rigid slumps, are generated using the 3D non-hydrostatic model NHWAVE; and (iii) the CVV sources are modeled as subaerial flows of a heavy fluid, using a 3D Navier-Stokes model. For each source, tsunami propagation to the USEC is then modeled in a series of nested grids of increasingly fine resolution, by one-way coupling, using FUNWAVE-TVD, a nonlinear and dispersive (2D) Boussinesq model. High-resolution inundation maps have been developed based on these results, so far for about a third of the USEC. A comparison of coastal inundation from each tsunami source shows similar alongshore patterns of higher and lower inundation, whatever the initial source direction; this is due to wave focusing and defocusing effects induced by the shelf bathymetry. Once developed for the entire USEC, inundation maps will fully quantify coastal hazard from the selected PMTs and allow developing site-specific mitigation measures and evacuation plans. Besides maximum inundation, other “products” available at high-resolution are maximum momentum flux, currents, and vorticity, although these are not systematically developed as maps in this phase of work.

INTRODUCTION

Since 2010, under the auspice of the US National Tsunami Hazard Mitigation Program (NTHMP; <http://nthmp.tsunami.gov/index.html>), the authors have performed tsunami modeling work to develop high-resolution tsunami inundation maps for the US east coast (USEC), starting with the most critical or vulnerable areas, but eventually to

¹To appear in *Proc. COPRI Coastal Structures and Solutions to Coastal Disasters Joint Conf. 2015*

²Department of Ocean Engineering, University of Rhode Island, Narragansett, RI 02882, USA; grilli@oce.egr.edu; agrilli@egr.uri.edu

³Center for Applied Coastal Research, University of Delaware, Newark, DE 19716, USA; btrad@udel.edu; kirby@udel.edu

cover the entire coast. These first generation maps are constructed as envelopes of maximum inundation caused by the most extreme near- and far-field tsunami sources, a.k.a., Probable Maximum Tsunamis (PMTs), both historical and hypothetical, in the Atlantic Ocean basin, without considering their return period or probability. Probabilistic tsunami hazard analyses may be part of future generations of inundation maps.

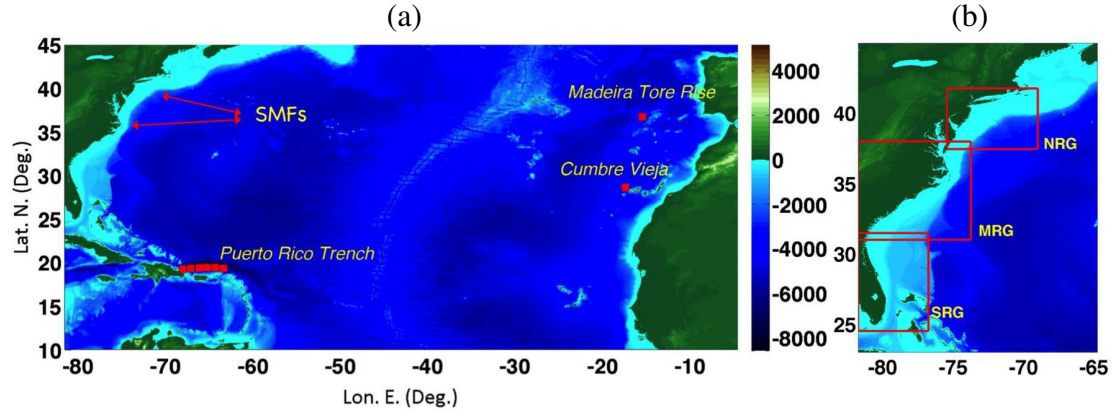


Figure 1: (a) Locations of near- and far-field tsunami sources in Atlantic Ocean, and footprint and ETOPO1 bathymetry (m) of FUNWAVE-TVD’s 1 arc-min grid G1; (b) zoom-in on USEC, with footprints of 3 regional 20 arc-sec nested grids G2 (NRG, MRG, SRG).

Tsunami sources leading to the PMTs included (Fig. 1a; see also ten Brink et al., 2008): (i) *far-field seismic* sources : (1) a series of M_w 9 sources in the Madeira Tore Rise, representing possible sources of the 1755 Lisbon earthquake (LSB), and (2) a M_w 9 source in the Puerto Rico Trench (PRT; e.g., Grilli et al., 2010), corresponding to an entire failure of the 600 km long trench; (ii) *extreme flank collapses* (80 or 450 km³ volume) of the Cumbre Vieja Volcano (CVV) on La Palma (Canary Islands; e.g., Abadie et al., 2012; Tehranirad et al., 2015); and (iii) *near-field Submarine Mass Failures* (SMFs) on or near the USEC continental shelf break. Areas prone to tsunami-genic SMFs were first identified based on Monte Carlo slope stability analyses (Grilli et al., 2009), which showed that SMF tsunami hazard is highest north of Cape Hatteras, a region where USGS identified and parameterized numerous SMF scars from historical SMFs on the continental shelf and shelf break (ten Brink et al., 2014), with the most prominent one being the historical 165 km³ Currituck (CRT) underwater landslide (Geist et al., 2009; Grilli et al., 2015a). Based on a geotechnical analysis of site specific data, 4 areas deemed at higher SMF risk and having sufficient sediment accumulation for a large SMF (Fig. 2) were selected for analysis. According to the PMT approach used in first-generation maps, SMF tsunami sources in these 4 areas were modeled with the approximate geometry (volume, dimensions, depth) of the CRT slide in a site specific orientation: these are referred to as SMF CRT proxy tsunami sources.

METHODOLOGY

Tsunami propagation model

Tsunami propagation from each source to the USEC was modeled using the nonlinear and dispersive two-dimensional (2D) Boussinesq long wave model (BM) FUNWAVE-TVD, in a series of nested grids of increasing resolution, by a one-way

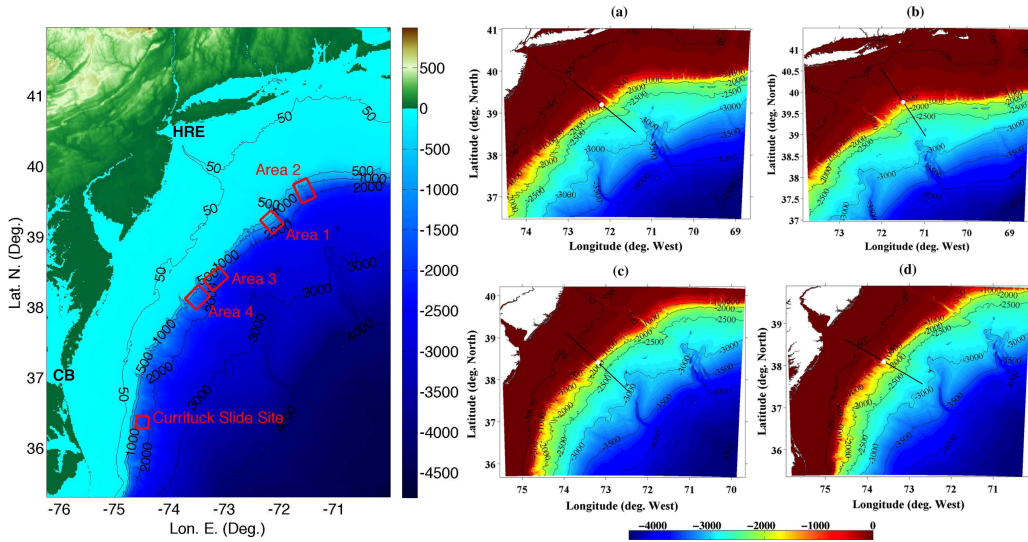


Figure 2: Left: Locations of historical CRT slide complex and of 4 areas where CRT SMF proxies are sited. Right: location and direction of motion of SMF proxies sited in areas 1-4 (subplots a-d); each subplot represents the footprint of the NHWAVE grid used to simulate the SMF tsunami sources. Color scales are bathymetry/topography in meter.

coupling method. FUNWAVE-TVD is a newer implementation of FUNWAVE (Wei et al., 1995), which is fully nonlinear in Cartesian grids (Shi et al., 2012) and weakly nonlinear in spherical grids (Kirby et al., 2013). The model was efficiently parallelized for use on a shared memory cluster (over 90% scalability is typically achieved), which allows easily using large grids. FUNWAVE and then FUNWAVE-TVD have been widely used to simulate tsunami case studies (e.g., Grilli et al., 2007; Ioualalen et al., 2007; Tappin et al., 2008, 2014; Abadie et al., 2012; Tehranirad et al., 2015; Grilli et al., 2010, 2013, 2015a,b). As discussed in introduction, since 2010, the authors have used this model and related methodology to compute tsunami inundation maps for the USEC, as part of the NTHMP work (e.g., Abadie et al., 2012; Grilli and Grilli, 2013a; Grilli et al., 2015; Tehranirad et al., 2015; see <http://chinacat.coastal.udel.edu/nthmp.html>) and also for several other tsunami hazard assessment studies of coastal nuclear power plants in the U.S. Both spherical and Cartesian versions of FUNWAVE-TVD were validated through benchmarking and approved for NTHMP work (Tehranirad et al., 2011).

As they include frequency dispersion effects, BMs simulate more complete physics than models based on Nonlinear Shallow Water Equations (NSWE), which until recently were traditionally used to simulate co-seismic tsunami propagation. Dispersive models are necessary to accurately simulate landslide tsunamis, which are typically made of shorter and hence more dispersive waves than co-seismic tsunamis (Watts et al., 2003). However, dispersion is also important for modeling propagation and coastal impact of co-seismic tsunamis, since undular bores can occur near the crest of incident long waves, in increasingly shallow water (Madsen et al., 2008). The importance of dispersion for modeling tsunami propagation was confirmed by running FUNWAVE in both BM and NSWE modes, by Tappin et al. (2008) for the 1998 Papua New Guinea landslide tsunami, and by Ioualalen et al. (2007) for the 2004 Indian Ocean and Kirby et al. (2013) for the 2011 Tohoku, coseismic tsunamis.

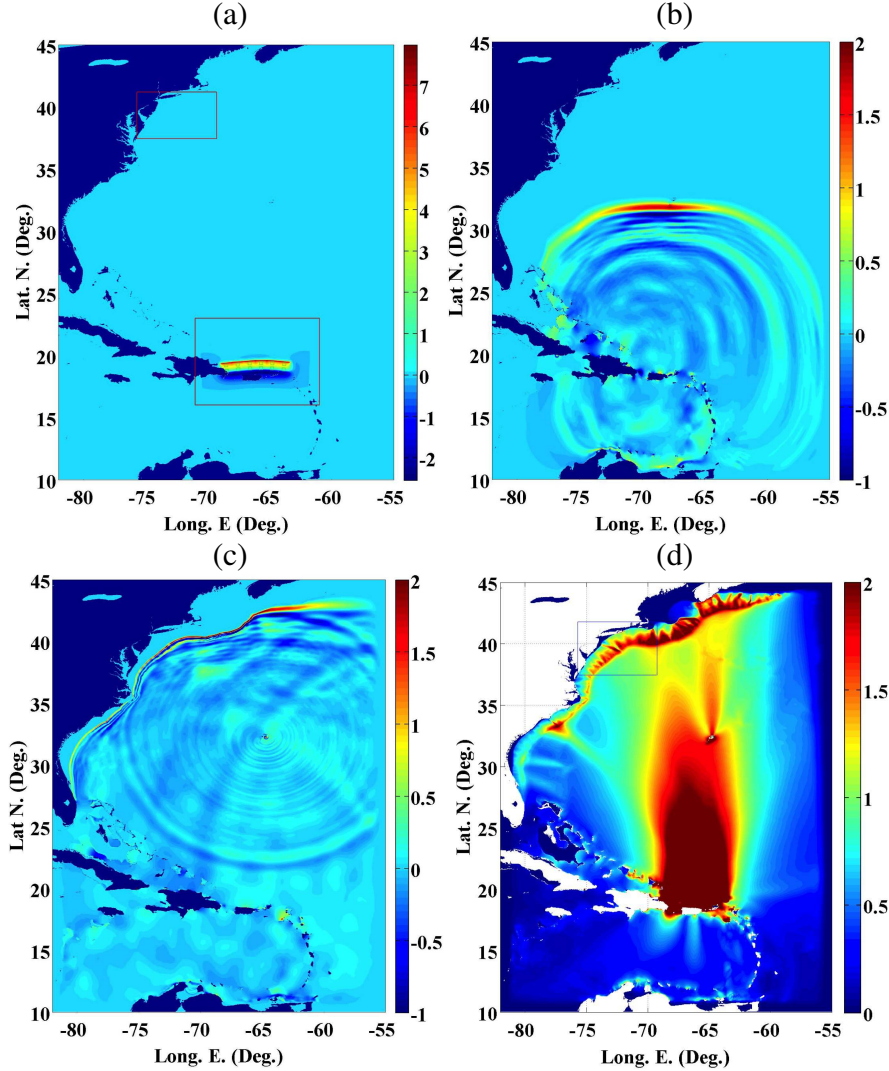


Figure 3: Simulations with FUNWAVE-TVD of the Mw 9 PRT seismic source in 1 arc-min grid G1 (truncated at Lon. E. -55; Fig. 1a): (a) Initial surface elevation of tsunami source computed in lower red box with Okada’s (1985) method, based on 12 SIFT sub faults (Gica et al., 2008; Grilli et al. 2013b); the upper red box is the area of the 20 arc-sec nested grid G2-NRG (Figs. 1b, 6); (b,c) instantaneous surface elevations after $t = 1\text{h } 42\text{ min}$ and $3\text{h } 20\text{ min}$ of propagation; (d) envelope of maximum surface elevation over a 6h simulation. Color scales are surface elevation in meter.

Simulations of tsunami propagation are performed in nested grids (Figs. 1, 3a), using a one-way coupling method, in which time series of surface elevation and depth-averaged current are computed for a large number of stations/numerical wave gages, defined in a coarser grid, along the boundary of the finer grid used in the next level of nesting. Computations are fully performed in the coarser grid and then are restarted in the finer grid using the station time series as boundary conditions. As these include both incident and reflected waves computed in the coarser grid, this method closely approximates open boundary conditions. It was found that a nesting ratio with a factor 3-4 reduction in mesh size allowed achieving good accuracy in tsunami simulations. Note that to prevent reflection in the first grid level, sponge layers are used along all the

offshore boundaries.

For the 3 far-field sources (LSB, PRT, CVV), simulations are initiated in a 1 arc-min (about 1800 m) resolution ocean basin scale spherical grid G1, covering the footprint of Fig. 1a (with 100 to 200 km wide sponge layers on offshore boundaries), in which tsunami sources are specified as initial conditions. The first level of nested grids are 3 regional 20 arc-sec (about 500-600 m) spherical grids G2, referred to as NRG, MRG and SRG (Fig.1b). For the near-field SMF sources, simulations are directly initiated in grids G2, based on sources computed with NHWAVE (see next section). To compute detailed inundation maps, tsunami simulations for all sources are continued in finer nested Cartesian grids of about 125, 30 and 10 m resolution. For each grid level, whenever possible, bathymetry and topography are interpolated from data of accuracy commensurate with the grid resolution. In deeper water, we use NOAA's 1 arc-min ETOPO-1 data (Fig. 1); in shallower water and on continental shelves, we use NOAA's NGDC 3" (about 90 m) and 1" (about 30 m) Coastal Relief Model data and, finally, onshore, we use NOAA's 10 m resolution tsunami DEMs, if available, or the equivalent FEMA data if not.

Along the shore, FUNWAVE-TVD has an accurate moving shoreline algorithm that identifies wet and dry grid cells. Bottom friction is modeled by a quadratic law with a constant friction coefficient. In the absence of more specific data we used the standard value $C_d = 0.0025$, which corresponds to coarse sand and is conservative as far as tsunami runup and inundation. Earlier work indicates that tsunami propagation results are not very sensitive to the friction coefficient values in deeper water, but that they are in shallower water; in particular, the modeled wave height decay over a wide shallow shelf is strongly affected by bottom friction (Tehrani-rad et al., 2015). Finally, dissipation from breaking waves is modeled using a front tracking (TVD) algorithm and switching to NSWEs in grid cells where breaking is detected (based on a breaking criterion). Earlier work shows that numerical dissipation in NSW models closely approximates the physical dissipation in breaking waves (Shi et al., 2012).

Tsunami source generation models

The initial surface elevation of far-field seismic sources (LSB, PRT) is specified in FUNWAVE-TVD (with no velocity) based on the co-seismic seafloor deformation computed using Okada's (1985) method, as a function of fault plane parameters (e.g., Fig. 3a, Fig. 4a,b,c); this is acceptable since water is nearly incompressible and raise times are usually small. Okada's method solves a three-dimensional (3D) elasticity problem for a homogeneous half-space with a dislocation specified over an oblique plane. Single or multiple fault planes can be used and for each of those the required parameters are the fault plane area (width W and length L), depth d at the source centroid, centroid location (lat-lon), 3 angles for orientation of the fault plane (dip, rake, strike) and the shear modulus (μ) of the medium (10-60 Gpa, for shallow rupture in soft/poorly consolidated marine sediment to deep rupture in basalt). The moment magnitude of the anticipated earthquake is defined as M_o (J) = μLWS , where S denotes fault slip. Therefore, besides the geometrical and material parameters, to complete the source parameterization, one needs either the slip value or the M_o value of the considered event (or its magnitude, $M_w = (\log M_o)/1.5 - 6$, on a base 32 log scale).

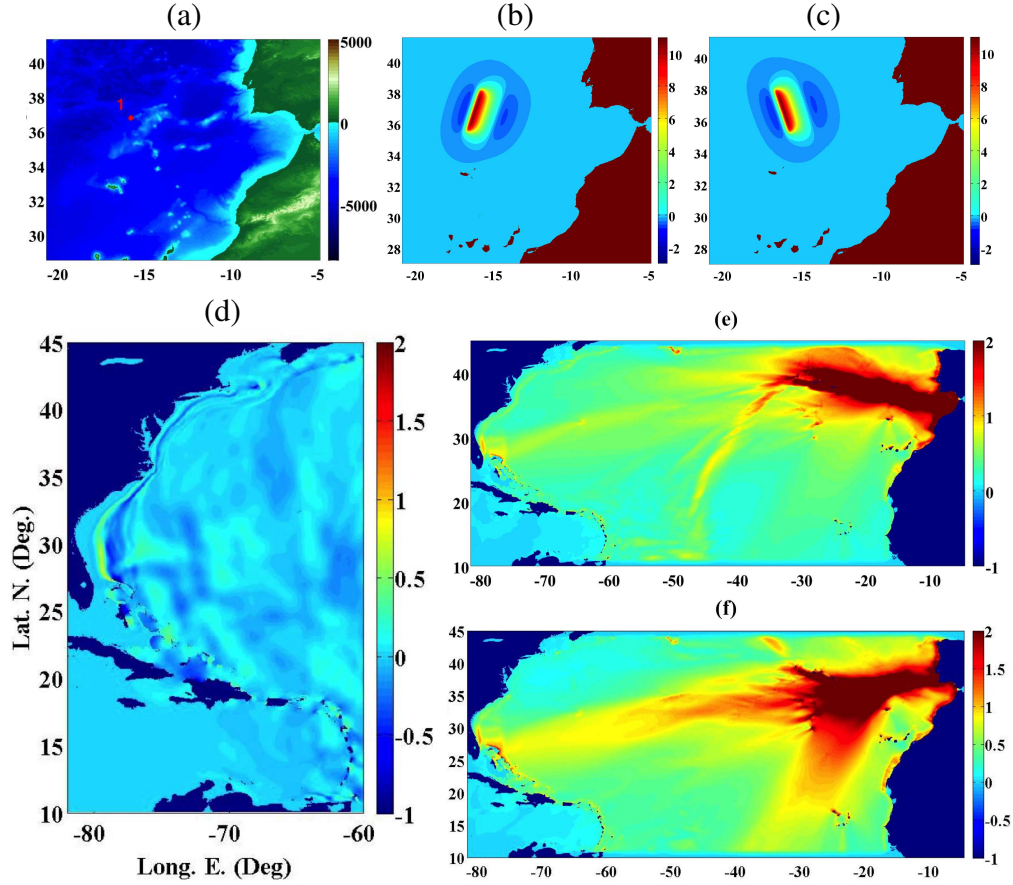


Figure 4: Simulations with FUNWAVE-TVD of the Mw 9 LSB seismic source in 1 arc-min grid G1: (a) Close-up of Madeira Trench Rise (1) with bathymetry/topography (m); (b,c) initial tsunami surface elevation computed with Okada's (1985) method, for 15 and 345 deg. strike, respectively (Grilli and Grilli, 2013a); (d) instantaneous surface elevation after $t = 6\text{h } 30\text{ min}$ of propagation; (e,f) envelope of maximum surface elevation over a 9h simulation for (b) and (c), respectively. Color scales are surface elevation in meter.

The far-field source for the CVV flank collapse is computed using the 3D multi-material Navier-Stokes model THETIS, as a subaerial slide represented by a heavy Newtonian fluid of density 2.9 (see details in Abadie et al., 2012). Once the slide has stopped moving and most of its energy has been transferred to the water motion, surface elevation and depth-averaged currents are re-interpolated into a FUNWAVE-TVD horizontal grid of 1000 m resolution, to further compute tsunami propagation, and then at $t = 20\text{ min}$ into the event, into grid G1.

Finally, for near-field SMF sources, tsunami generation is computed with the 3D non-hydrostatic model NHWAVE, using a 500 m resolution Cartesian horizontal grid and a coarse vertical grid made of a few boundary fitting (sigma) layers; 3 to 5 such layers are usually sufficient to achieve a good accuracy (Ma et al., 2012). Here, all CRT SMF proxies are assumed to be rigid slumps, which is conservative as far as tsunami generation, with their geometry and kinematics specified as bottom boundary condition in NHWAVE, from the parameters of the CRT slide (see details in Grilli et al., 2015a).

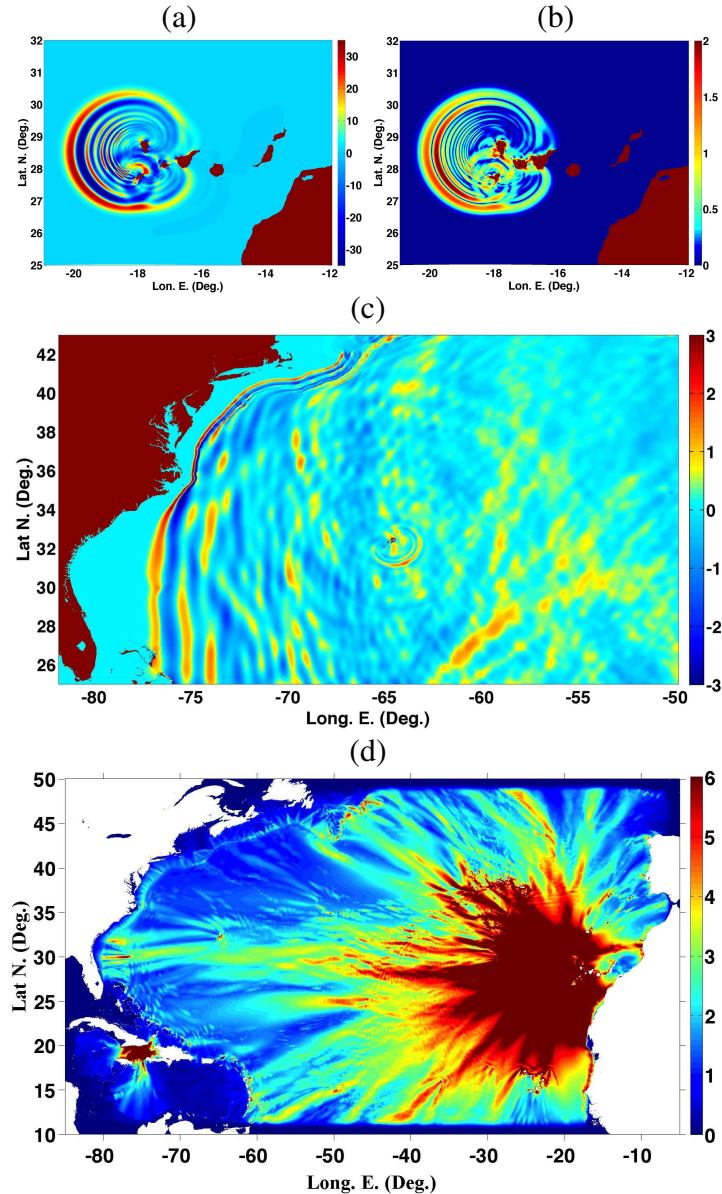


Figure 5: Simulations with FUNWAVE-TVD of the 80 km^3 CVV flank collapse source in grid G1 (Fig. 1a): (a,b) Initial surface elevation (m) and horizontal velocity module (m/s) of tsunami source at $t = 20$ min; (c) Instantaneous surface elevation after $t = 8$ h; (d) envelope of surface elevation over 10 h. Color scales are surface elevation (meter).

RESULTS

Source parameters, tsunami generation, and oceanic propagation

Here, we give results of the parametrization, initialization and initial propagation in FUNWAVE-TVD's 1 arc-min grid G1, of the three far-field sources (PRT, LSB and CVV), and of the four CRT SMF proxy sources in 20 arc-sec grids G2 (Fig. 1). For a historical case such as LSB, the source is based on both the estimated magnitude and location/geometry of the failure. The largest hypothetical earthquake in a subduction zone such as PRT can be inferred from potential slip estimated as the convergence rate (e.g., mm/year) times the number of years considered for the event return period. With this approach, Grilli et al. (2010) for instance found that a M_w 9.1 PRT earthquake

corresponds to a 600 year return period, while a M_w 8.1 earthquake to only 40 years. For the CVV flank collapse, we considered both the most extreme scenario of 450 km³ and the most probable extreme scenario of 80 km³ (Abadie et al., 2012; Tehranirad et al., 2015). As indicated before, the near-field SMF sources are parameterized as CRT proxies, sited in areas 1 to 4 in Fig. 2. Details of parameterization, tsunami generation, and initial oceanic propagation for each source are given in the following.

Far-field PRT source. As in Grilli et al. (2010), we are modeling an extreme $M_w = 9$ seismic source in the PRT, corresponding to the entire trench rupturing north of Puerto Rico (Figs. 1a, 3a), over a 600 km length. Unlike in this earlier work, where only one fault plane was used, to better model the curved geometry of the trench, we use 12 individual sub-fault planes with parameters obtained from the SIFT data base (“Short-term Inundation Forecast for Tsunamis”; Gica et al., 2008). Each sub-fault is thus a “SIFT-unit source” of magnitude $M_w = 7.5$, length $L = 100$ km, width $W = 50$ km, with a 1 m slip; with these parameters, we find $\mu = 35.6$ GPa. Moreover the location, depth and orientation of each subfault plane (strike, dip and rake angles) is based on the local geology (see details in Grilli and Grilli, 2013b). The slip of each subfault is then scaled for the total magnitude to be $M_w = 9$, or $M_o = 3.162 \cdot 10^{22}$ J; thus, $S = (M_o/12)/(LW\mu) = 14.8$ m. Using these parameters in Okada’s model, we find the initial surface elevation shown in Fig. 3a, which varies between -6 and +8 m. Figs. 3b and c show instantaneous surface elevations computed in grid G1 with FUNWAVE-TVD after 1h 42 min and 3h 20 min of propagation, respectively, and Fig. 4d shows the envelope of maximum surface elevations, over 6h of simulations. Results show a fairly narrow and directional train of the largest tsunami waves aimed almost directly north (towards the upper USEC), with elevations of order 2 m, and some westward propagation affecting the lower USEC, but to a lesser extent, with elevations of order 1 m. The detailed near-field impact of this source in Puerto Rico and Hispaniola was detailed in Grilli et al. (2010) and Grilli et al. (2015b), respectively.

Far-field LSB sources. The exact location and parameters of the 1755 LSB event (Fig. 1a), which is the basis for this M_w 9 seismic source, are unknown. As part of the NTHMP work, Grilli and Grilli (2013a) modeled a dozen sources of this magnitude, sited at various locations in the Açores convergence zone, with parameters selected based on earlier published work. Strike angle, in particular, which strongly affects the tsunami directionality, was varied to cause maximum impact on various sections of the USEC. They found that maximum impact on the USEC was created by sources sited in the Madeira Tore Rise (Fig. 4a), which is the westernmost potential site for the historical earthquake. Parameters of the fault plane are (Barkan et al., 2008): (i) fault plane center: -10.753 E Lon. 36.042 N Lat., (ii) $L = 317$ km, (iii) $W = 126$ km, (iv) dip angle: 40 deg., (v) rake angle: 90 deg., (vi) strike angle: 15 to 345 deg.; (vii) $S = 20$ m, and (viii) $\mu = 40$ GPa, which yields $M_o = 3.162 \cdot 10^{22}$ J or $M_w = 9$. All other parameters being equal, Grilli and Grilli (2013a) found that a strike angle of 15 deg. led to the maximum impact on the upper USEC, while an angle of 345 deg. caused maximum impact on the lower USEC and in the Carribeans and Hispaniola. Figs. 4b and c show the two seismic sources based on these parameters and 2 strike angles, respectively, computed with Okada’s model; we see an over 10 m initial surface elevation. Fig. 4d shows the instantaneous surface elevation for the first

source, simulated with FUNWAVE-TVD in grid G1, after 6h 30 min of propagation, and Figs. 4e and f show the envelopes of maximum surface elevations obtained for each source, over 9h of simulations. Maximum tsunami impact clearly has the expected directionality for both sources, but overall (in this coarse grid) maximum onshore elevations are only up to 1 m along the USEC.

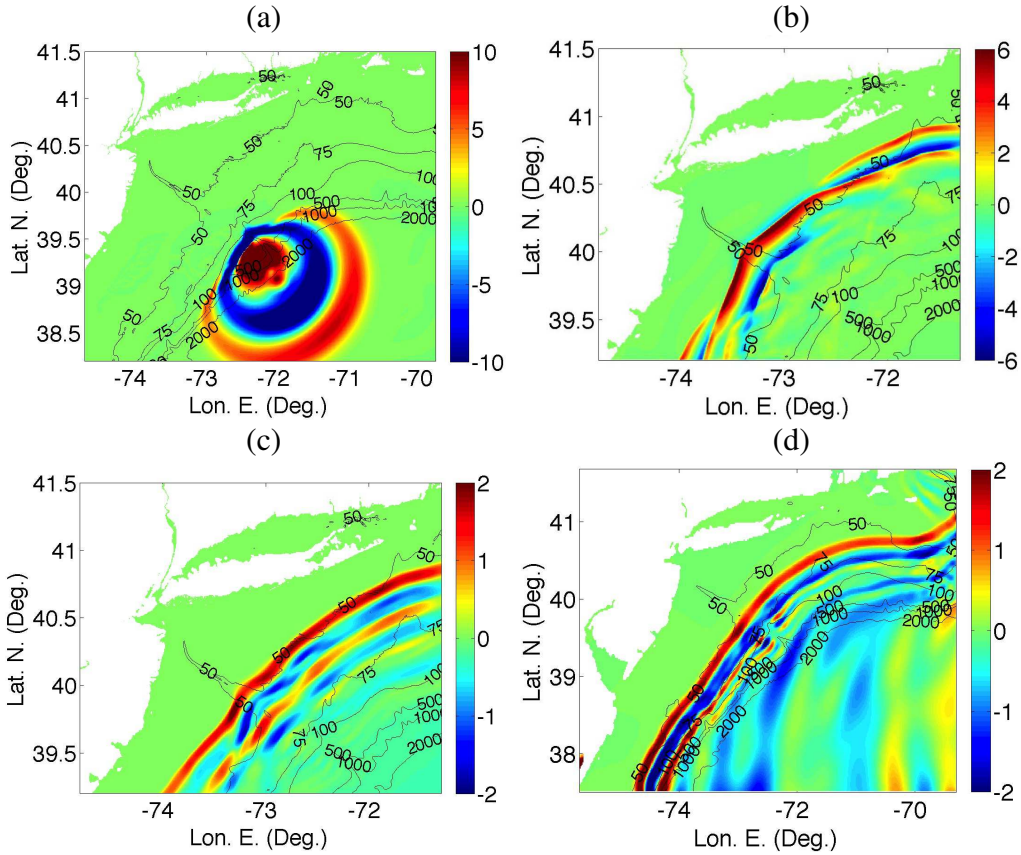


Figure 6: Instantaneous surface elevations of the CRT SMF proxy in Area 1 (Fig. 2) computed in 20 arc-sec grid G2-NRG (Figs. 1b, 3a): (a) with NHWAVE at $t = 13$ min; and (b) with FUNWAVE-TVD at $t = 1$ h 18 min. Instantaneous surface elevation computed in grid G2 with FUNWAVE-TVD for the : (c) PRT tsunami at $t = 4$ h; (d) CVV tsunami at $t = 8$ h. Color scale is elevation and black contour bathymetry, both in meter.

Far-field volcanic collapse sources (CVV). The surface elevation and velocity of the 80 km^3 CVV flank collapse source (from Abadie et al., 2012) are shown in Figs. 5a,b, 20 min after the event; at that time, we see a concentric wave train with elevations ranging between -35 and +35 m, velocity modules up to 2 m/s, and a clear directionality in the WSW direction. Fig. 5c shows the instantaneous surface elevation computed with FUNWAVE-TVD in grid G1, 8h into the event. Despite the long propagation distance, very large waves with elevations in the range -3 m to +3 m are approaching the USEC. Fig. 5d shows the envelope of maximum surface elevations computed over 10h of simulations; in this coarse grid, most of the USEC would experience over 3 m nearshore surface elevations. [It should be noted that the very large elevations in (d,e) west of Hispaniola are spurious and due to grid coarseness; these disappear in finer nested grids.] Maximum impact occurs in Cape Hatteras and Florida, but in the latter

location, there appears to have large wave decay over the wide shelf. Tehranirad et al. (2015) showed that this is essentially an effect of bottom friction. Note that results for the 450 km³ CVV (not detailed here), are qualitatively similar to those of the smaller source, except that elevations are about 3 times larger (see Abadie et al., 2012 and Tehranirad et al., 2015 for details).

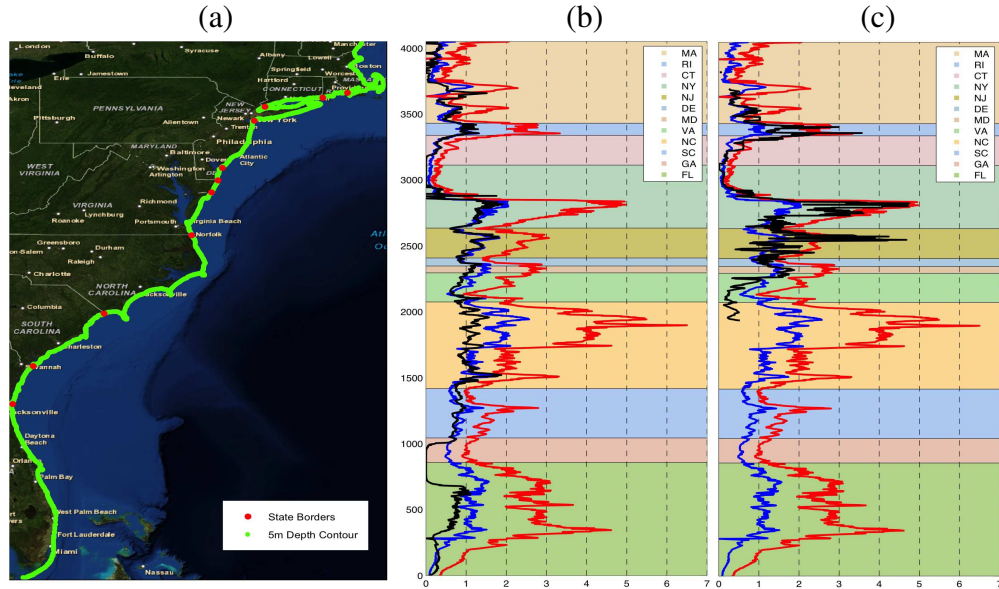


Figure 7: Maximum surface elevations (b,c, x-axis in meter) computed at 5 m depth with FUNWAVE-TVD, as a function of distance along the USEC (b,c, y-axis in km; states identified in (a) by colors), for the CVV tsunami, from the 80 (blue) and 450 (red) km³ sources, compared to the: (b) PRT; and (c) CRT SMF proxy (Area 1), tsunamis (black).

Near-field SMF sources. Grilli et al. (2015a) modeled each of the CRT SMF proxy sources sited in Areas 1 to 4 (Fig. 2) in 3D using NHWAVE. They determined that all the wave generation was completed before 13.3 min and hence at that stage reinterpolated the computed surface elevation and depth-averaged velocity into FUNWAVE-TVD grids to continue the simulations. We proceed similarly here and Fig. 6a shows the initial surface elevation computed with NHWAVE for the SMF in Area 1, interpolated into the 20 arc-sec G2-NRG grid (Fig. 1b); elevations at this stage range between -10 and +10 m and there are two main trains of waves, propagating on-shore and offshore, respectively. Fig. 6b then shows instantaneous surface elevations computed with FUNWAVE-TVD for this case, after 1h 18 min.

Nearshore tsunami propagation and coastal impact

For each tsunami source, the nearshore propagation is simulated with FUNWAVE-TVD in a series of nested grids of increasingly fine resolution. Figs. 6b,c and d, for instance compare the surface elevations simulated in the 20 arc-sec grid G2-NRG (Fig. 1b) for the CRT SMF proxy (Area 1), PRT, and CVV tsunamis, respectively. We see that, despite the very different sources for these three cases and their widely different locations (i.e., nearshore, south and east of the considered area), all tsunami wave trains, due to refraction over the wide shallow shelf, are nearly aligned with the 50 m isobath and start focusing away from the Hudson River canyon, and onto the western

Long Island and northern New Jersey shores.

This focusing-defocusing behavior is also quite apparent in the envelopes of maximum surface elevations in Figs. 3d, 4e,f and 5d, for the PRT, LSB and CVV tsunamis, respectively, and more clearly illustrated in Fig. 7, which plots the maximum surface elevations computed at a 5 m depth off the USEC, as a function of the distance along shore, for the PRT and CRT SMF proxy (area 1), as compared to the CVV 80 and 450 km³ cases. Despite large differences in elevation magnitude, we see very similar along-shore patterns of elevation/inundation for all tsunami sources. Hence, there is a strong control of the bathymetry on tsunami coastal impact; Tehranirad et al. (2015) further illustrated the latter for the CVV tsunamis by drawing incident wave rays.

Results of detailed simulations of tsunami inundation in nested grids, developed into 10 or 30 m resolution inundation maps, are left out due to lack of space.

CONCLUSIONS

We presented the methodology for and overall results of modeling work conducted to simulate tsunami hazard along the USEC. Based on this work, many tsunami inundation maps have been developed, so far for the most critical areas of the USEC, but eventually for the entire coast. Detailed reports on the latter and actual maps can be found on the project webpage at: <http://chinacat.coastal.udel.edu/nthmp.html>.

Acknowledgments The authors gratefully acknowledge support from the National Tsunami Hazards Mitigation Program grants NA14NWS4670041 and NA15NWS4670029.

REFERENCES

- Abadie, S., J.C. Harris, S.T. Grilli and R. Fabre (2012). "Numerical modeling of tsunami waves generated by the flank collapse of the Cumbre Vieja Volcano (La Palma, Canary Islands): tsunami source and near field effects," *J. Geophys. Res.*, 117, C05030.
- Barkan, R., ten Brick, U.S., Lin, J. (2008). "Far field tsunami simulations of the 1755 Lisbon earthquake: Implication for tsunami hazard to the U.S. East Coast and the Caribbean," *Marine Geol.*, 264, 109-122.
- Gica, E., M. C. Spillane, V. V. Titov, C. D. Chamberlin, and J. Newman (2008). "Development of the forecast propagation database for NOAAs Short-Term Inundation Forecast for Tsunamis," *NOAA Tech. Memo. OAR PMEL-139*.
- Grilli A.R. and S.T. Grilli (2013a). "Modeling of tsunami generation, propagation and regional impact along the U.S. East Coast from the Azores Convergence Zone," *Research Report no. CACR-13-04*, 20 pp, University of Delaware. <http://www.oce.uri.edu/grilli/grilli-grilli-cacr-13-04>.
- Grilli A.R. and S.T. Grilli (2013b). "Modeling of tsunami generation, propagation and regional impact along the upper U.S East coast from the Puerto Rico trench," *Research Report no. CACR-13-02*, 18 pp., University of Delaware <http://www.oce.uri.edu/grilli/grilli-grilli-cacr-13-02>.
- Grilli, A.R., Grilli S.T., David, E. and C. Coulet (2015b). "Modeling of tsunami propagation in the Atlantic Ocean Basin for tsunami hazard assessment along the North Shore of Hispaniola," In *Proc. 25th Offshore and Polar Engng. Conf. (ISOPE15, Kona, HI, USA. June 21-27, 2015)*, 733-740.
- Grilli, S.T., Ioualalen, M, Asavanant, J., Shi, F., Kirby, J. and Watts, P. (2007). "Source Constraints and Model Simulation of the December 26, 2004 Indian Ocean Tsunami," *J. Waterway Port Coast. Oc. Engng.*, 133(6), 414-428.

- Grilli, S.T., S. Dubosq, N. Pophet, Y. Prignon, J.T. Kirby and F. Shi (2010). "Numerical simulation and first-order hazard analysis of large co-seismic tsunamis generated in the Puerto Rico trench: near-field impact on the North shore of Puerto Rico and far-field impact on the US East Coast," *Nat. Haz. Earth Syst. Sc.*, 10, 2109-2125.
- Grilli, S.T., J.C. Harris, T. Tajalibakhsh, T.L. Masterlark, C. Kyriakopoulos, J.T., Kirby and F. Shi (2013). "Numerical simulation of the 2011 Tohoku tsunami based on a new transient FEM co-seismic source: Comparison to far- and near-field observations," *Pure Appl. Geophys.*, 170, 1333-1359.
- Grilli S.T., O'Reilly C., Harris J.C., Tajalli-Bakhsh T., Tehranirad B., Banihashemi S., Kirby J.T., Baxter C.D.P., Eggeling T., Ma G. and F. Shi (2015a). "Modeling of SMF tsunami hazard along the upper US East Coast: Detailed impact around Ocean City, MD," *Nat. Haz.*, 76(2), 705-746.
- Ioualalen, M., Asavanant, J., Kaewbanjak, N., Grilli, S.T., Kirby, J.T. and P. Watts (2007). "Modeling the 26th December 2004 Indian Ocean tsunami: Case study of impact in Thailand," *J. Geophys. Res.*, 112, C07024.
- Kirby, J.T., Shi, F., Tehranirad, B., Harris, J.C. and S.T. Grilli (2013). "Dispersive tsunami waves in the ocean: Model equations and sensitivity to dispersion and Coriolis effects," *Ocean Modell.*, 62, 39-55.
- Ma G., Shi F., Kirby J.T. (2012). "Shock-capturing non-hydrostatic model for fully dispersive surface wave processes," *Ocean Modell.*, 43, 2235.
- Madsen P.A., D.R. Fuhrman and H. A. Schaffer (2008) "On the solitary wave paradigm for tsunamis," *J. Geophys. Res.*, 113, C12012.
- Okada, Y. (1985). "Surface deformation due to shear and tensile faults in a half space," *Bull. Seismol. Soc. America*, 75(4), 1135-1154.
- Shi, F., J.T. Kirby, J.C. Harris, J.D. Geiman and S.T. Grilli (2012). "A High-Order Adaptive Time-Stepping TVD Solver for Boussinesq Modeling of Breaking Waves and Coastal Inundation," *Ocean Modell.*, 43-44, 36-51.
- Tappin, D.R., Watts, P., S.T. Grilli (2008). "The Papua New Guinea tsunami of 1998: anatomy of a catastrophic event," *Nat. Haz. Earth Syst. Sc.*, 8, 243-266.
- Tappin D.R., Grilli S.T., Harris J.C., Geller R.J., Masterlark T., Kirby J.T., F. Shi, G. Ma, K.K.S. Thingbaijam, and P.M. Maig (2014). "Did a submarine landslide contribute to the 2011 Tohoku tsunami ?" *Mar. Geol.*, 357, 344-361.
- Ten Brink, U., Twichell D., Geist E., Chaytor J., Locat J., Lee H., Buczkowski B., Barkan R., Solow A., Andrews B., Parsons T., Lynett P., Lin J., and M. Sansoucy (2008). "Evaluation of tsunami sources with the potential to impact the U.S. Atlantic and Gulf coasts," *USGS Administrative report to the U.S. Nuclear Regulatory Commission*, 300 pp.
- Tehranirad B., Harris J.C., Grilli A.R., Grilli S.T., Abadie S., Kirby J.T. and F. Shi (2015). "Far-field tsunami impact in the north Atlantic basin from large scale flank collapses of the Cumbre Vieja volcano, La Palma," *Pure Appl. Geophys.*, 28pp. doi:10.1007/s00024-015-1135-5 (published online 07/21/15).
- Tehranirad, B., Shi, F., Kirby, J. T., Harris, J. C. and Grilli, S. (2011). "Tsunami benchmark results for fully nonlinear Boussinesq wave model FUNWAVE-TVD, Version 1.0," *Research Report No. CACR-11-02*, University of Delaware.
- Watts P., Grilli S.T., Kirby J.T., Fryer G.J. and D.R. Tappin (2003) "Landslide tsunami case studies using a Boussinesq model and a fully nonlinear tsunami generation model," *Nat. Haz. Earth Syst. Sc.*, 3, 391-402.
- Wei, J., Kirby, J.T, Grilli, S.T. and Subramanya, R. (1995). "A Fully Nonlinear Boussinesq Model for Surface Waves. Part 1. Highly Nonlinear Unsteady Waves," *J. Fluid Mech.*, 294, 71-92.